Wavelength calibration of spectra measured by the Global Ozone Monitoring Experiment: variations along orbits and in time

Jos H.G.M. van Geffen

Royal Netherlands Meteorological Institute (KNMI)
P.O. Box 201, 3730 AE De Bilt, The Netherlands

Published in: *Applied Optics* **43**, pp. 695–706, 2004.

Abstract

The nadir-viewing Global Ozone Monitoring Experiment (GOME) spectrometer aboard the second European Remote Sensing satellite (ERS-2) measures spectra in the range 240–790 nm. For the near-real time delivery of ozone columns and profiles at KNMI, a wavelength calibration method was developed which allows for a variation in both location and width of the spectral bins along the detector. The resulting wavelength grid of earthshine spectra varies along an orbit. This variation shows a correlation with instrument temperatures for a window around 306 nm; for other wavelength windows there is no correlation. The wavelength grid of calibrated solar spectra shows fluctuations without an apparent pattern and no correlation with instrument degradation.

OCIS codes: 010.1290, 120.6200, 280.0280, 300.6170.

1. Introduction

The Global Ozone Monitoring Experiment (GOME) is a nadir-viewing ultraviolet and visible spectrometer aboard the second European Remote Sensing satellite (ERS-2). GOME measures spectra in four spectral channels between 240 and 790 nm (see Table 1) of sunlight scattered in the atmosphere and reflected by the surface of the Earth. Once a day a direct solar spectrum is measured in these four channels for radiometric calibration. ERS-2 was launched by the European Space Agency (ESA) in 1995 and orbits Earth at an altitude of about 790 km in a sun-synchronous polar orbit. Each orbit takes about 100 minutes and ERS-2 completes 14 orbits per day. The satellite crosses the equator at 10:30 a.m. local time when going north to south.

The largest off-nadir scan angle of GOME's scan mirror is about 30°, giving a full swath width of around 960 km at ground level and global coverage in three days. In the direction of flight each ground pixels measures 40 km. GOME's scan mirror performs a 4.5-second forward scan from east to west, with respect to the direction of flight, followed by a 1.5-second backscan from west to east. The forward scan is divided into three 1.5-second scan pixels: east, centre and west, where the centre (or: nadir) pixel is directly below the satellite.

Table 1 *Wavelength ranges of the four detector channels of the GOME instrument, the approximate detector pixel size and the spectral resolution of GOME for each channel. The last column shows the number of data points (detector pixels) for each channel.*

channel	wavelength range	pixel size	resolution	#points
1	237 – 315 nm	0.11 nm	0.17 nm	695
2	313 – 405 nm	0.12 nm	0.17 nm	841
3	407 – 608 nm	0.22 nm	0.30 nm	1024
4	599 – 794 nm	0.22 nm	0.35 nm	1024

Detector channels 1 and 2 (Table 1) are for earthshine spectra divided into two bands ('a' and 'b'); channels 3 and 4 not. The wavelength of the division point between bands 1a and 1b has been changed once since the launch of ERS-2: initially the division was around 307 nm, since June 1998 it is around 283 nm. Band 1a has an integration time of 12 seconds, in order to improve the signal-to-noise ratio, as the spectral signal for these short wavelengths is relatively weak due to strong absorption by ozone. The eight times larger integration time of band 1a thus comprises two full scans, each with three forward and one backscan ground pixel, which implies that a measurement corresponds to a ground pixel of about 960 by 100 km. For more information on the GOME instrument, the reader is referred to Ref. 1-3 and references therein.

In order to facilitate a near-real time delivery (that is: within 3 to 6 hours after observation) of ozone data, a GOME Fast Delivery Service (FDS) is set up at the Royal Netherlands Meteorological Institute (KNMI), in collaboration with ESA. The FDS provides total ozone columns, vertical ozone profiles, assimilated ozone fields, UV index forecasts, and cloud data via the World Wide Web (`http://www.knmi.nl/gome_fd/`). For this service, KNMI receives parts of the raw (level-0) GOME spectra via ftp: the so-called Extracted GOME Instrument header (EGOI) data, used by ESA to monitor the status of the GOME instrument.[4,5]

The raw data in these EGOIs contains the spectral measurements of nine selected wavelength windows, listed in Table 2, providing enough data to retrieve ozone columns and vertical ozone profiles with sufficient accuracy. EGOI window 6 is the "ozone DOAS window" (Differential Optical Absorption Spectroscopy) from which the total ozone column can be retrieved.[4,6] Windows 1 through 6 are used for the retrieval of ozone profiles.[7] The measurements in windows 7 and 8 are used for the correction of the polarisation sensitivity of the instrument. Window 9 contains the oxygen-A band, which is used for the retrieval of cloud fraction and cloud top height. In the FDS, the latter is done with the Fast Retrieval Scheme for Cloud Observables[8,9] (FRESCO).

A number of steps has to be performed to convert the raw level-0 data in the EGOI files into spectral level-1 data.[10] One of these steps is a wavelength calibration, which attributes a wavelength value to each detector pixels using a high-resolution solar spectrum as reference spectrum. The wavelength calibration method has been designed specifically for the FDS, *i.e.* for the nine EGOI windows

Table 2 *Definition of the nine EGOI windows since June 1998, used for the near-real time FDS at KNMI as outlined in the Introduction. The fourth column lists the number of data points (detector pixels) in each window, which totals to 445. Apart from these nine windows, the EGOI data contain all instrument health parameters, such as system temperatures, and polarisation information.*

window	wavelength range	width	#points	band
1	272.16 – 275.91 nm	3.75 nm	35	1a
2	282.93 – 285.55 nm	2.62 nm	25	1b
3	292.51 – 302.96 nm	10.45 nm	98	1b
4	305.31 – 307.87 nm	2.56 nm	25	1b
5	311.92 – 314.46 nm	2.54 nm	25	1b
6	323.13 – 336.22 nm	13.09 nm	116	2b
7	351.64 – 352.76 nm	1.12 nm	11	2b
8	372.32 – 373.42 nm	1.10 nm	11	2b
9	758.00 – 778.50 nm	20.50 nm	99	4

listed in Table 2, to provide spectra that are sufficiently accurately calibrated to retrieve ozone columns and vertical ozone profiles. The method is, however, not restricted to these windows: it can in principle be used for any high-resolution spectrometer in any wavelength window within an available reference spectrum.

The method of this wavelength calibration is described in detail by Van Geffen and Van Oss,[11] together with a discussion of the accuracy and some examples. Section 2 of the present paper briefly describes the wavelength calibration, in particular the aspects relevant for the subjects of the remainder of the paper: the variation of the results of the calibration of earthshine spectra — the change in wavelength assigned to a detector pixel with respect to an arbitrary initial wavelength guess — along GOME's orbits and from orbit to orbit.

Section 3 describes the data used in this analysis. Investigated is whether the variation shows a correlation with one of the instrument temperatures. Due to a temperature dependence of some of the optical components of the instrument, namely, there are variations in instrument temperatures along an orbit and from orbit to orbit, as discussed in Section 4. The orbital variation of the calibration results and the correlation with instrument temperature variations are presented in Section 5.

Apart from a variation in the calibration results along and between successive orbits, there is also a variation in time over a much longer period. Due to the orbital variation of the earthshine spectrum results, these spectra are not suited for a study of year-to-year variations. Hence, measured solar spectra covering a period of almost six years are used for this study, as described in Section 6. Some concluding remarks are given in Section 7.

2. The wavelength calibration method

The method of the wavelength calibration, developed for the wavelength windows available for the FDS, employs a high-resolution solar spectrum[12] as a reference spectrum and performs a non-linear fit of two parameters: a shift and a squeeze, with respect to some initial wavelength grid, thus allowing for a variation in both the location and the width of the spectral bins along the detector. The method determines the shift and squeeze, and hence the wavelength grid, that has the smallest (χ^2) difference between the measured and a simulated GOME spectrum. The latter is constructed from the instrument slit function[13] and a reference spectrum; the resolution of the slit function used in the present paper is given in the fourth column of Table 1. In this Section the wavelength calibration method and its accuracy are described briefly; a more detailed description and discussion is given by Van Geffen and Van Oss.[11]

2.1 The wavelength grid

The wavelength grid used in the calibration method is, for a given channel, given by a fifth-degree polynomial:

$$\lambda(j) = a_1 + a_2 j + a_3 j^2 + a_4 j^3 + a_5 j^4 \ , \tag{1}$$

where $\lambda(j)$ is the wavelength at the centre of detector pixel j, with $j = 0$ for the first pixel and $j = M - 1$ for the last pixel of the channel under consideration, with M the number of detector pixels of the channel given in the last column of Table 1. This parametrisation is sufficient to describe GOME's wavelength grid.

The wavelengths $\lambda(j)$ of Eq. (1) form for a certain set of coefficients a_k the initial guess of the wavelength grid of the spectrum in the window to be calibrated. The shift (α, a wavelength increment with dimension nm) and squeeze (β, a dimensionless factor) that follow from the wavelength calibration adjust the first two coefficients and thus form a new wavelength grid:

$$\lambda'(j) = (a_1 + \alpha) + (a_2\beta) j + a_3 j^2 + a_4 j^3 + a_5 j^4 \ . \tag{2}$$

Due to the presence of a squeeze factor, the change of wavelength with respect to the initial wavelength grid is different for each detector pixel:

$$\Delta\lambda(j) = \lambda'(j) - \lambda(j) = \alpha + a_2(\beta - 1) j \ , \tag{3}$$

with the combination ($\alpha = 0, \beta = 1$) representing no change in the wavelength grid.

For the FDS, the initial wavelength grid is based on a set of arbitrary but realistic coefficients, one set for each individual window. Because the initial wavelength grids are an arbitrary choice, the absolute values of the shift and squeeze found by the calibration have no physical meaning. But since the calibration of a given wavelength window always starts from the same initial grid, it is possible to compare the calibration results, for example, for ground pixels along an orbit or between successive orbits (geographically or in time), as is the focus of the present paper.

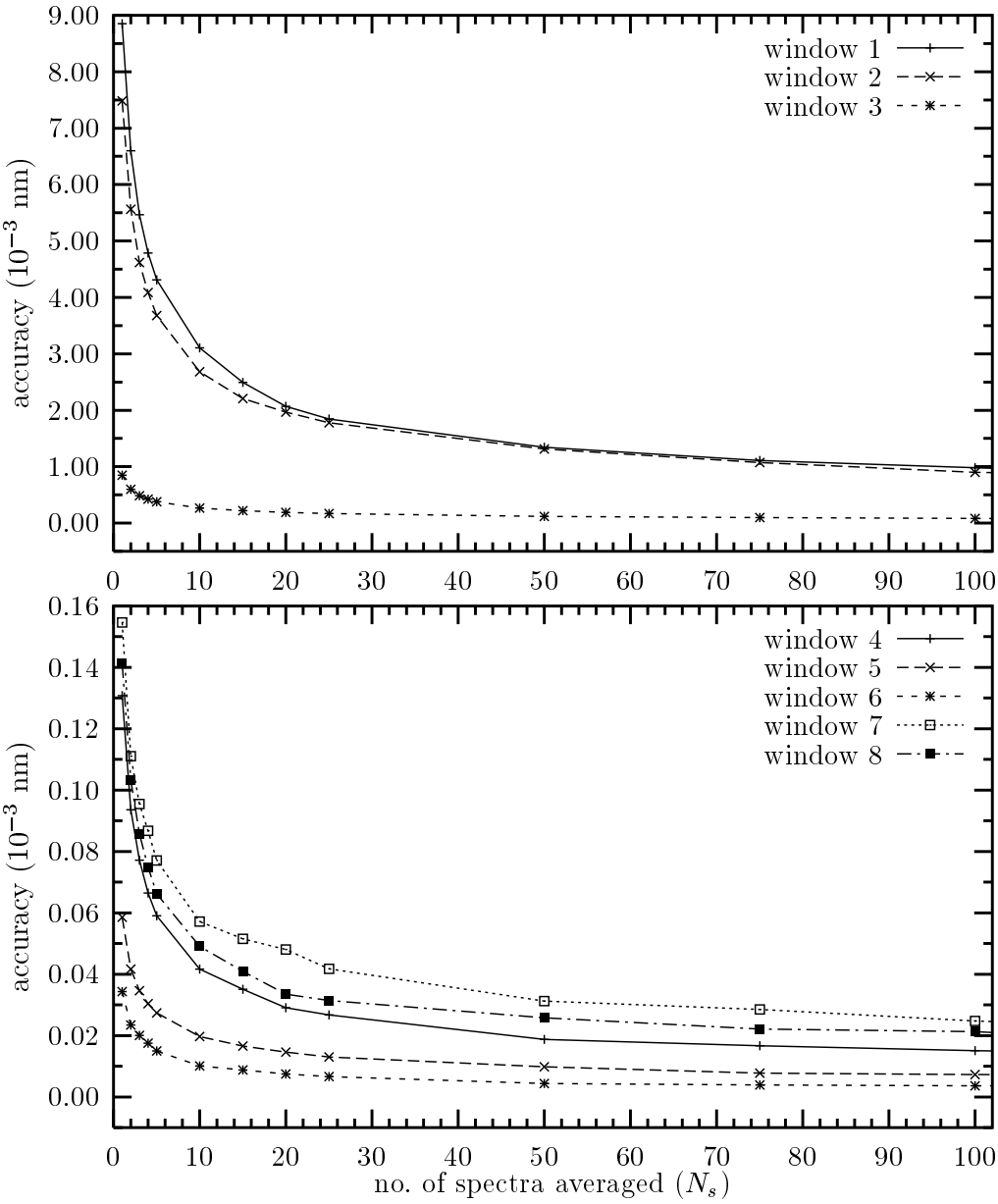

Figure 1 *Accuracy, given in* 10^{-3} nm, *for windows 1 through 8 as function of the number of spectra averaged, as determined by Van Geffen and Van Oss.*[11] *Note the different scales in the two panels.*

2.2 The accuracy of the method

The accuracy of the wavelength calibration method is limited by the accuracy of the reference spectrum (which is 0.002 nm for wavelengths below 300 nm and 0.001 nm above that[12]); and by the quality of the measured spectrum. The accuracy is determined by Van Geffen and Van Oss[11] using simulated GOME earthshine spectra and is shown to depend strongly on the signal-to-noise ratio of the spectra. That ratio can be improved by averaging a set of N_s spectra before the wavelength calibration, where the averaging should be done over consecutively measured spectra.

Figure 1 shows the accuracy for windows 1 through 8 in units of 10^{-3} nm as

function of N_s. Clearly, the accuracy improves with increasing N_s. The calibration in windows 1, 2 and 3 is much less accurate than in the other windows due to the lower signal-to-noise ratio. The calibration in windows 7 and 8 is less accurate than in windows 4–6 because these two windows have fewer data points (*cf.* Table 2). The accuracy of window 9 cannot be determined in the same way but is expected to be at least as good as the accuracy for the windows in channel 2.

As discussed below, the calibration results vary along an orbit. This implies that the value of N_s should not be too large, otherwise the calibration becomes less accurate again. Averaging over 20 spectra for windows 1 and 2, as is done in the FDS, gives an accuracy of 0.002 nm; this is sufficient for the retrieval of ozone profiles.[14] An averaging over 10 spectra is performed in the FDS for the other wavelength windows, not to improve the accuracy but to save computational time in view of the constraint of the near-real time delivery of the data.

2.3 Recalibration of GDP level-1 spectra

Though designed for use with the nine EGOI windows of the FDS listed in Table 2, the wavelength calibration method is not limited to these windows: it can in principle be used with any wavelength window within the range of the reference spectrum (which in this case covers GOME's four channels). This makes the method suitable for use with any high-resolution (ir)radiance spectrometer, such as the Scanning Imaging Absorption Spectrometer for Atmospheric Cartography [SCIAMACHY, aboard ESA's Environmental Satellite (ENVISAT); launched in 2002], the Ozone Monitoring Instrument [OMI, aboard Earth Observing System (EOS) Aura; to be launched in 2004], and GOME-2 [aboard the Meteorological Operational Satellite (METOP); to be launched in 2005].

Solar and earthshine spectra, the so-called level-1 data, are official product release of the GOME Data Processor (GDP) of the ESA Processing and Archiving Facility at Deutsches Zentrum für Luft- und Raumfahrt (DLR) in Oberpfaffenhofen, Germany, together with some level-2 data, *e.g.* the total column of ozone and NO_2, and cloud information.[2,13,15]

The wavelength calibration of these GDP-made spectra appears to be insufficiently accurate for example for the retrieval of ozone profiles, as described by Van Geffen and Van Oss.[11] The calibration method can be used also to recalibrate the wavelength grid of GDP level-1 spectra. This has been implemented in a software package called GomeCal, together with an improved polarisation correction[16] and a radiometric recalibration[17,18] the latter includes a correction for the degradation of the GOME instrument, which is apparent since 1998 (see also Section 6). The GomeCal package is briefly introduced by Van Geffen and Van Oss[11] and is made available via the World Wide Web (`http://www.knmi.nl/gome_fd/gomecal/`). For details on usage, the reader is referred to the GomeCal documentation,[19] which is also available on-line.

3. Data used in the analysis of earthshine spectra

The wavelength calibration method is applied to earthshine spectra measured by GOME to investigate the variation of the wavelength change which results from the calibration along an orbit and from orbit to orbit. Variations in the wavelength grid along an orbit may be correlated to changes in some instrument temperatures.[1] For the analysis the data available for the FDS, *i.e.* the nine EGOI windows listed in Table 2, are used because instrument temperature information is available in the EGOI data files, and not in the GDP-made level-1 data files.

As mentioned in the Introduction, earthshine spectra in band 1a have an integration time of 12 seconds, whereas the integration time of the other bands is 1.5 seconds. Due to this 12-second integration time, there are about 210 spectra of window 1 available per orbit. The integration covers eight ground pixels, starting with an east pixels and ending with a backscan pixel. The spectrum of window 1 is for the analysis simply attributed to the last backscan ground pixel used in the integration; spectra of the other ground pixels are skipped.

The data used for the analysis with earthshine spectra are the orbits of 1, 2 and 3 March 2000, when orbits give measurements between about 70° N and 70° S. On these three days ERS-2 made 14, 15 and 14 orbits, respectively, on the day-side of the Earth and GOME scanned with normal (full) swath width along all orbits. The data set does not contain small swath or nadir-static scans, nor does it contain spectra with integration times longer than the standard 12 or 1.5 second scans.

For the analysis, the spectra of windows 1 and 2 are averaged over $N_s = 20$ spectra and the spectra of windows 3 through 9 over $N_s = 10$ spectra, where running average is used with a step of 5 spectra. For windows 1 and 2 this means an average over spectra 1–20, 6–25, 11–30, etc., and for windows 3 through 9 over spectra 1–10, 6–15, 11–20, etc. (The averaging over 20 and 10 spectra, respectively, is the same as in the FDS, but there it is a simple average, not a running average.)

4. Instrument temperatures

The temperature of the GOME instrument is monitored at several locations within the instrument and these temperatures are available in the (level-0) EGOI data files (not in the GDP level-1 data files). For each earthshine spectrum there is one set of instrument temperatures. Changes in some of these temperatures along an orbit may affect the measurement, which could show up as changes along an orbit in the wavelength calibration. A description of the instrument systems is given in Refs. 1,3.

One of the key elements in the optical system of GOME is a quartz predisperser prism. The refractive index of quartz depends not only on the wavelength of the light passing through it, but also on the temperature of the prism. In fact the predisperser prism is the most temperature sensitive element of the optical system.[1]

Figure 2 shows the predisperser prism temperature of orbit 1 of 1 March 2000 (dashed line) and a running average through these data (solid curve), as function

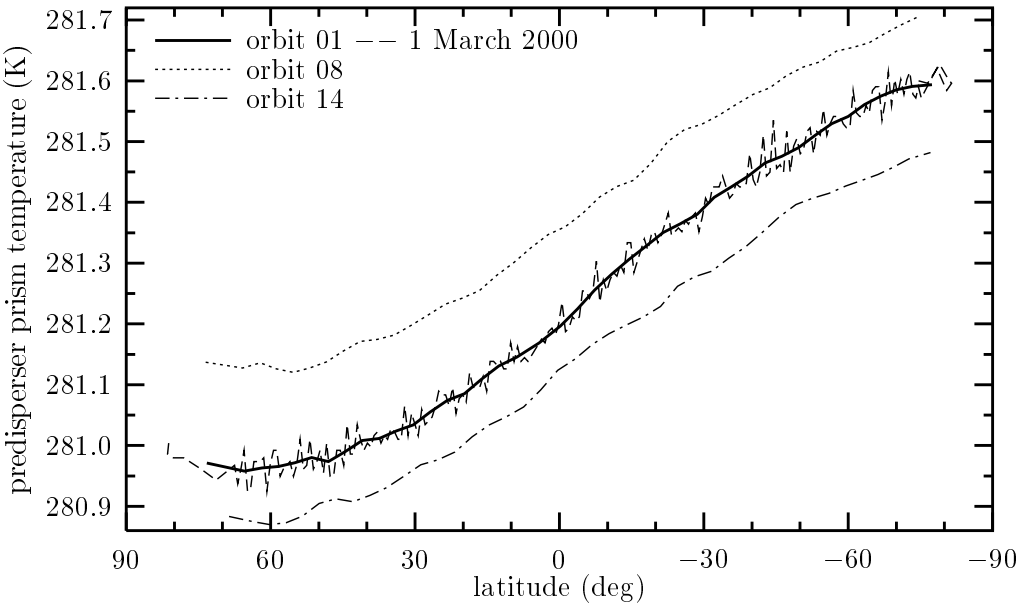

Figure 2 *Temperature of the predisperser prism along selected orbits of 1 March 2000 while the satellite moves from north to south on the day-side of the Earth, as function of latitude. For orbit 1 both the true temperatures (dashed line) and a running average (solid line) are shown. For orbits 8 and 14 only a running average is plotted. The curves of the other orbits of the same day are similar in shape and fall between those of orbits 8 and 14.*

of latitude, *i.e.* along the orbit. The running average is over 10 measurements with a step of 5, hence over measurements 1–10, 6–15, 11–20, etc. Clearly, the temperature increases as the satellite moves along its orbit, partly because the satellite is warmed up by the sun and partly because light passes through the instrument. Different orbits of the same day show temperature curves of the same shape, but at a higher or lower temperature level. This is illustrated in Figure 2 by curves of the running averages of the temperatures of orbits 8 and 14. For the other orbits of 1 March 2000, the curves fall between these two curves.

Temperature curves for the orbits of 2 and 3 March 2000 are similar to those in Figure 2, but at different temperature levels. Figure 3 shows for the three days the predisperser prism temperature as function of longitude, for three selected latitudes: $+60^{\circ}$, 0°, and -60°. The values plotted are interpolated from running averages over the data of the respective orbits, and each symbol marks an orbit. The temperatures at 3 March are clearly systematically about 0.1 K below those of 1 March. The temperatures of 2 March are in between these two, with the temperature of orbit 14 about equal to the temperature of orbit 1.

There appears to be a maximum in the temperature of the predisperser prism over the Atlantic Ocean, for orbit 8 (dotted line in Figure 2 and filled circles in Figure 3) or orbit 9, while above the Pacific Ocean there seems to be a minimum, superimposed on the general feature that the temperature increases as the instrument goes southward along the orbits.

At first sight there is no reason to expect a difference between successive orbits in the instrument temperatures. Over a period of only three days there is

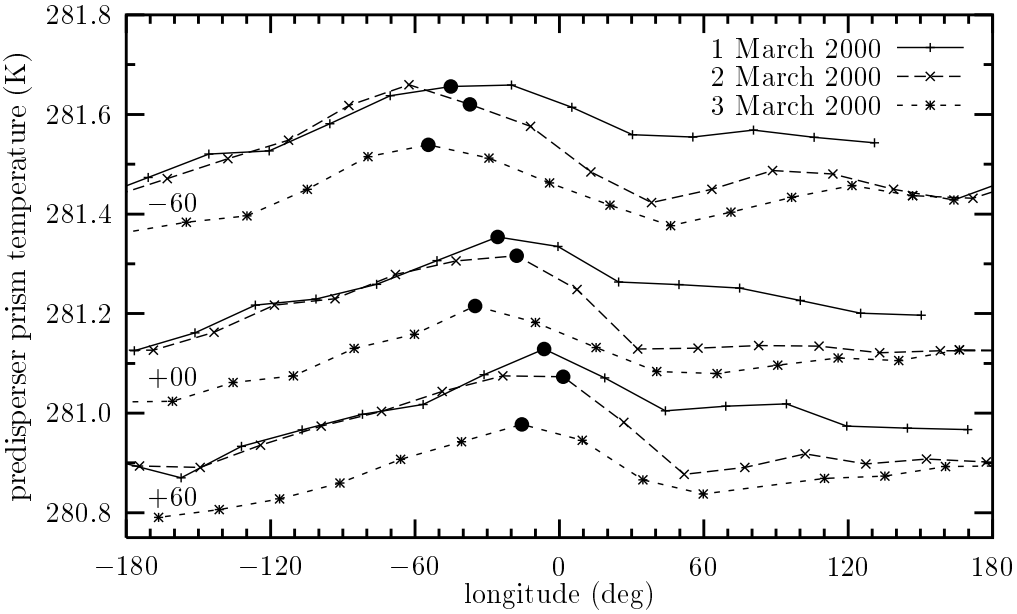

Figure 3 *Temperature of the predisperser prism for the orbits of 1, 2 and 3 March 2000 as function of longitude for three selected latitudes: +60° (bottom three curves), 0° (middle three curves) and −60° (top three curves). The right most points of the 1 March curves (solid lines) are those of orbit 1 of that day; the temperature curve as function of latitude for that orbit is given by the solid line in Figure 2. The filled circle at each curve marks orbit 8 of the three days. (Orbit 4 of 3 March has no point on the +60° curve, due to lack of data.)*

no significant differences to be expected in the way the instrument warms in the sun while the satellite orbits the Earth: as the satellite is in a sun-synchronous orbit, it passes the latitudes each orbit at the same local time.

Perhaps the differences in temperatures are due to varying activity of other satellite instruments aboard ERS-2. Atmospheric conditions, such as the presence of clouds, affect the intensity of the earthshine radiance, and this may influence the warming of the instrument. The cloud fraction and cloud top height derived with the FRESCO algorithm,[8,9] however, give no indication of a cloud-related effect. To investigate this matter further requires studying more days than the three considered here, which falls outside the scope of the present paper.

The temperature of several other components of the instrument are also measured and most of these show a variation along an orbit as in Figure 2, with a different temperature level. The temperature of the centre of the optical bench, for example, is always about 1.05 K lower than the predisperser prism temperature. The orbit-to-orbit variation of these temperatures is similar to the variation shown in Figure 2.

The temperatures measured at several points at the Detection and Data Handling Unit of GOME show a similar trend, but with a larger increase along an orbit (1.5 K instead of about 0.6 K) and initially a steeper increase than the curves shown in Figure 2. The temperature of two other elements show a very different behaviour along an orbit: the sun diffuser and the cooler radiator. It is unlikely, though, that either of these temperature variations affects the results of

the wavelength calibration of the earthshine spectra.

The temperatures of the detectors themselves, the Focal Plane Assemblies (FPAs), are measured at eight points per channel. These FPA temperatures show some fluctuations around a mean value (about 235.0 K). Most of these fluctuations are about ± 0.1 K, but there are some peaks of ± 0.2 K. There is no dependence visible on the position along an orbit, nor is there a clear difference between successive orbits (the variation of a running average between orbits is also about 0.1 K). Hence, no effect of the FPA temperatures on a variation in the wavelength calibration along an orbit or from orbit to orbit is expected.

In short, if there is a correlation between the results of the wavelength calibration and the variation of a system temperature, the temperature of the predisperser prism serves as a good proxy.

5. Calibration results of earthshine spectra

The results of the wavelength calibration of a spectrum in a given window can be characterised by the change in wavelength of the data point in the middle of the wavelength window: $\Delta\lambda(i_m)$. As the initial grid is an arbitrary (but realistic) choice, the absolute value of $\Delta\lambda(i_m)$ has no physical meaning, but the relative variation along an orbit and between orbits does. This means that $\Delta\lambda(i_m)$ can be offset by a constant value (different for each window) to make an analysis easier.

The wavelength change is different for different windows, different orbits and different days. To ease the following discussion, three indices are introduced to $\Delta\lambda$ and the i_m-index is dropped: $\Delta\lambda(n_w, n_o, n_d)$, with n_w the number of the wavelength window and n_o the number of the orbit on day n_d of March 2000. The latter two indices are also given to the predisperser prism temperature: $T(n_o, n_d)$. Let furthermore $C(n_w, n_o, n_d)$ represent the coefficient of correlation between $\Delta\lambda(n_w, n_o, n_d)$ and $T(n_o, n_d)$ for a given data set $\{n_w, n_o, n_d\}$. Gaps in the curves of $\Delta\lambda$ along an orbit in the graphs shown below are due to gaps in the level-0 date delivery.

The following discussion first focuses on wavelength window 4, because the variation along the orbit and a possible correlation with the temperature of the predisperser prism can be discussed easiest for this window. As is shown, there is for individual orbits some degree of (anti-)correlation between the predisperser prism temperature and the wavelength change which results from the calibration, but this correlation is not so clearly present when comparing the results of different orbits. For the other wavelength windows (5–9 and 1–3) there is no significant correlation between the calibration results of these windows and the temperature of the predisperser prism.

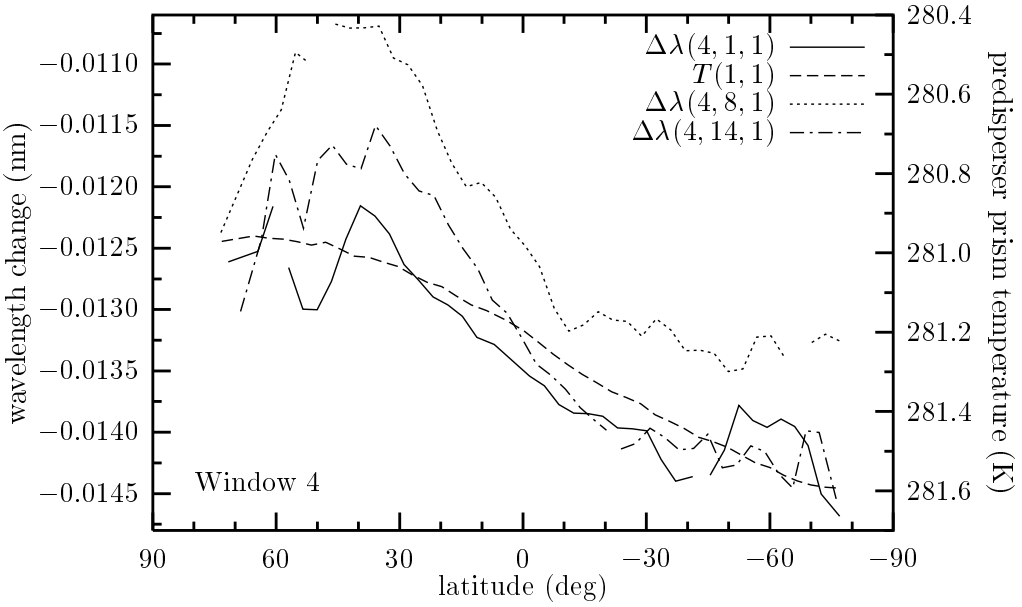

Figure 4 *Wavelength change* $\Delta\lambda(4, n_o, 1)$ *as a result of the wavelength calibration (left axis) of window 4 along orbits* $n_o = 1$, 8 *and* 14 *of 1 March 2000, as function of latitude. Plotted is also the temperature of the predisperser prism* $T(n_o, 1)$ *given by the solid line in Figure 2 (right axis). The accuracy of the calibration method for window 4 is better than* 0.0001 nm *(cf. Figure 1).*

5.1 Wavelength window 4

Figure 4 shows for window 4 the wavelength change $\Delta\lambda(4, n_o, 1)$ for orbits 1, 8 and 14 of 1 March 2000. Also plotted is the predisperser prism temperature $T(1, 1)$, with temperature increasing downward (right axis, dashed line). There is a clear negative correlation between $\Delta\lambda(4, 1, 1)$ and $T(1, 1)$ between $+40^o$ and -40^o latitude; over the full orbit $C(4, 1, 1) = -0.920$. The correlation for the other two orbits shown in Figure 4 are similar: $C(4, 8, 1) = -0.903$ and $C(4, 14, 1) = -0.930$. The lowest correlation coefficient on this day is for orbit 4: $C(4, 4, 1) = -0.840$.

Although there is a clear correlation between $\Delta\lambda$ and T along a single orbit, this is not continued from orbit to orbit. One would expect that $\Delta\lambda(4, 8, 1)$ is for every latitude below $\Delta\lambda(4, 1, 1)$ as $T(8, 1) > T(1, 1)$ [see Figure 2], but Figure 4 shows that $\Delta\lambda(4, 8, 1)$ is well above $\Delta\lambda(4, 1, 1)$ throughout the orbit. Similarly, as $T(14, 1) < T(1, 1)$ [see Figure 2], one would expect $\Delta\lambda(4, 14, 1)$ to be above $\Delta\lambda(4, 1, 1)$, but that is true only for a part of the orbit. As for the other orbits, the $\Delta\lambda(4, n_o, 1)$-curves lie roughly between the curves of orbits $n_o = 1$ and $n_o = 8$. The correlation between $\Delta\lambda(4, n_o, 1)$ and $T(n_o, 1)$ over all 14 orbits of this day is therefore lower than for the individual orbits, namely: $C(4, \text{all}, 1) = -0.762$.

Plots of the same quantities of 2 and 3 March (not shown) display similar $\Delta\lambda$-curves and similar correlation coefficients for most orbits; a few of the orbits have coefficients of -0.6 and -0.7. An overview of all the correlation coefficients is given in the tables in the Appendix.

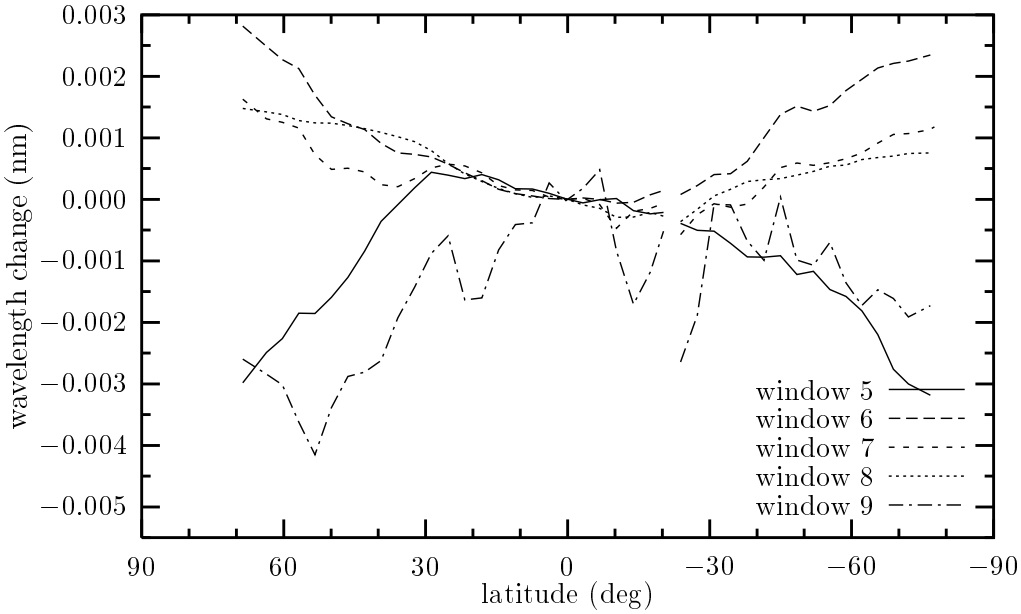

Figure 5 *Wavelength change* $\Delta\lambda(n_w, 14, 1)$ *as a result of the wavelength calibration of windows* $n_w = 5 - 9$ *along orbit 14 of 1 March 2000, as function of latitude. The curves have been offset with their value at the equator to get all curves within one graph. The accuracy of the calibration method for these windows is better than* 0.0001 nm *(cf. Figure 1). Note the lack of correlation with the temperature* T*, which is present in Figure 4 for window 4.*

5.2 Wavelength windows 5–9

The variation of $\Delta\lambda$ along an orbit for windows 5 through 9 is quite different from one another and from the variation for window 4 (Figure 4), as Figure 5 shows for orbit 14 of 1 March 2000. For the other orbits of the three days, the variation along the orbit is similar to the curves shown in Figure 5. For windows 5 through 8 the curves lie within 0.002 nm of one another. For $n_w = 9$ the variation along an orbit is more erratic, as the dash-dotted curve in Figure 5 indicates, and the differences between the orbits is bigger, namely up to 0.01 nm.

Comparing the curves in Figure 5 with the predisperser prism temperature in Figure 2 indicates that there is no significant correlation. The correlation coefficients are ± 0.6 for windows 8 and 9 along most orbits; for the other windows the correlation is worse. For some of the orbits on the three days the correlation coefficient is higher, up to 0.9. But on the whole the values of the correlation coefficient are very erratic, as the tables in the Appendix show.

Table 3 lists the frequency of the correlation coefficients gathered into 0.2 wide bins for all 43 orbits of 1–3 March put together. The high correlation for window 4, mentioned in the previous subsection, shows up clearly in this table. For windows 5–9 there is evidently no significant correlation between the temperature of the predisperser prism and the wavelength calibration. What is more, the not-significant correlation there is for the windows 6–8 in detector channel 2, is not of the same sign throughout the detector.

The wavelength change for windows 1–3, discussed in some detail in the next subsection, shows no significant correlation with the predisperser prism tempera-

Table 3 *Frequency of the coefficient of the correlation between the wavelength change $\Delta\lambda$ as a result of the wavelength calibration and the predisperser prism temperature T for all 43 orbits of 1–3 March 2000, for each of the nine wavelength windows n_w. The individual correlation coefficients are listed in the Appendix.*

correlation coefficient	n_w 1	2	3	4	5	6	7	8	9
−1.0 to −0.9	0	0	0	31	1	0	0	0	0
−0.9 to −0.7	0	2	7	9	0	0	0	6	0
−0.7 to −0.5	0	1	16	2	6	1	1	10	0
−0.5 to −0.3	0	6	11	0	10	1	8	10	2
−0.3 to −0.1	6	7	4	0	15	3	11	8	1
−0.1 to 0.1	5	10	4	1	8	6	14	5	3
0.1 to 0.3	11	4	0	0	2	11	7	3	2
0.3 to 0.5	10	8	1	0	1	10	1	0	17
0.5 to 0.7	7	3	0	0	0	7	1	0	11
0.7 to 0.9	4	2	0	0	0	4	0	1	6
0.9 to 1.0	0	0	0	0	0	0	0	0	1

ture either, though there is a tendency for a negative correlation for window 3.

Since the predisperser prism temperature was found to be a good proxy for variations in the system temperatures (Section 4), the conclusion must be that there is no correlation between the wavelength calibration and system temperatures, except for the small wavelength window $n_w = 4$ in detector channel 1.

5.3 Wavelength windows 1–3

Figure 6 shows the wavelength change $\Delta\lambda(1, n_o, 1)$ for window 1 along some orbits of 1 March 2000. The variation along orbit 1 of the wavelength change $\Delta\lambda(1, 1, 1)$ increase from about −0.0070 nm to about −0.0055 nm. Curves of the wavelength change of orbits 2–5 and 11–14 (not shown) have a similar variation along the orbit, within a 0.0030 nm wide band and no distinct peaks. Distinct peaks are visible in the wavelength change of windows 7–10, as is evident from Figure 6, but only in the latitude range −5° to −50°. The curve for orbit 6 (not shown) has a smaller peak, downward to about −0.012 nm between −20° and −30° latitude. Outside the ranges where these peaks occur, the curves of orbits 6–10 are similar to the curve of orbit 1.

On 2 and 3 March there are similar peaks in the wavelength change of window 1 for orbits passing through the same latitude-longitude range. This can be seen from Figure 7, which shows the wavelength changes $\Delta\lambda(1, n_o, n_d)$ along all orbits n_o of the three days $n_d = 1, 2, 3$ which exceed certain limits to show the distinct peak values in the calibration results. The region of these peaks in the wavelength change of window 1 is between −5° and −50° latitude, and between 0° and −90° longitude. This region corresponds roughly with what is known as the South Atlantic Anomaly, which is related to the Van Allen belts.

The Van Allen radiation belts are doughnut-shaped regions of high-energy charged particles trapped by the Earth's magnetic field. The inner radiation belt,

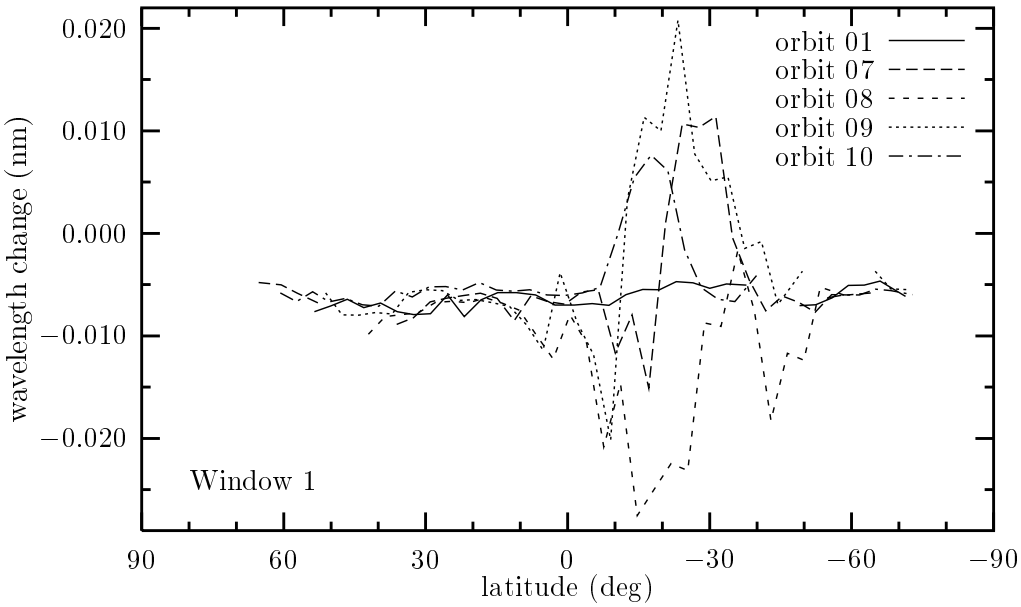

Figure 6 *Wavelength change* $\Delta\lambda(1, n_o, 1)$ *as a result of the wavelength calibration of window* $n_w = 1$ *along selected orbits on 1 March 2000, as function of latitude. The accuracy of the calibration method for window 1 is about* 0.002 nm *or better (cf. Figure 1).*

discovered by James Van Allen in 1958 with the Explorer 1 and 3 missions of NASA, occupies a relatively compact region above the equator roughly between 40° north and south. The Earth's magnetic dipole field is offset from its centre by about 500 km. As a result of this, the inner Van Allen belt is on one side closer to the Earth's surface. This region is named the South Atlantic Anomaly (SAA) and it lies roughly between latitudes −5° and −40°, and between longitudes −5° and −80°, *i.e.* a part of South America and the southern Atlantic Ocean.

Low-orbiting satellites, such as ERS-2, pass daily through the inner radiation belt in the SAA-region. Upon passing the inner belt, charged particles may impact on the GOME detector, causing higher-than-normal radiance values. The impact of charged particles on the GOME detectors decreases the quality of the measurements of earthshine spectra, notably in the UV (< 300 nm), as for these shorter wavelengths the signal-to-noise ratio is not high due to the small radiance values.

The peaks in the wavelength change over the SAA-region are an indication that the wavelength calibration is hampered by the peaks in the radiance values in this region. It may therefore be better to omit this region from the wavelength calibration and adopt, for example, the average results of the calibration between, say, +5° and +30° latitude of the orbit for the SAA-region. The limits for $\Delta\lambda$ used in the plot of Figure 7 could be employed as a kind of filter for the SAA-region. But as these limits are not based on a physical principle and thus rather arbitrary, it is better to simply use the latitude and longitude values of the SAA-region mentioned above as a filter, if the SAA-region has to be omitted.

The signal-to-noise ratio of the spectrum in window 2 is not as high as that in window 1 due to the shorter integration time at roughly the same radiance level.

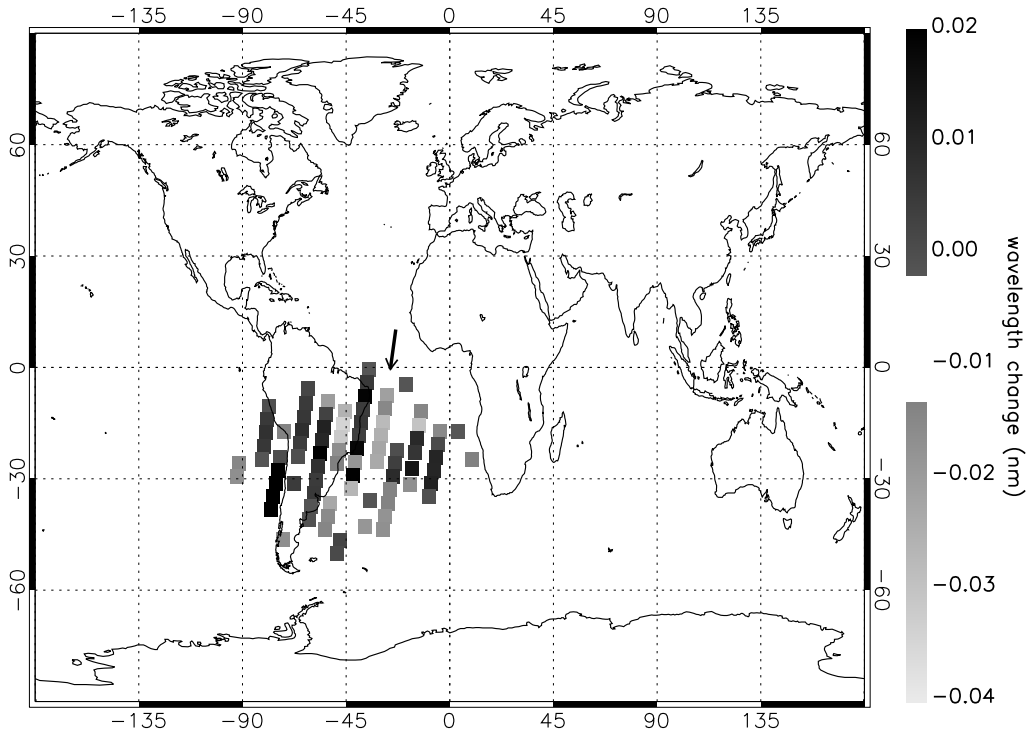

Figure 7 *Wavelength change $\Delta\lambda(1, n_o, n_d)$ as a result of the wavelength calibration of window 1 along all orbits of 1–3 March 2000, where each square represents a data point, not a ground pixel. Plotted are values of $\Delta\lambda$ larger than -0.002 nm and smaller than -0.013 nm. The arrow indicates orbit $n_o = 8$ of 1 March (cf. Figure 6); orbit 8 of 2 March is to the right of it, orbit 8 of 3 March to the left (cf. Figure 3).*

This reduced signal-to-noise ratio manifests itself as a considerable fluctuation of $\Delta\lambda(2, n_o, n_d)$ along an orbit, without a distinguishable increase or decrease with latitude. And the variation between successive orbits is of the same magnitude. The integration time for window 3 is as short as for window 2 but the radiance levels are higher and the window has more data points (Table 2), as a result of which the signal-to-noise ratio of window 3 is better than that of window 1. This difference in signal-to-noise ratio can also be seen from the standard deviation of a simple averaging over all $\Delta\lambda(n_w, n_o, n_d)$-values of all orbits of the three days per window:

$$\begin{aligned} \overline{\Delta\lambda(1, n_o, n_d)} &= -0.00692 \text{ nm} , \qquad \sigma(1) = 0.00462 \text{ nm} \\ \overline{\Delta\lambda(2, n_o, n_d)} &= -0.00120 \text{ nm} , \qquad \sigma(2) = 0.01072 \text{ nm} \\ \overline{\Delta\lambda(3, n_o, n_d)} &= -0.00861 \text{ nm} , \qquad \sigma(3) = 0.00147 \text{ nm} \end{aligned} \tag{4}$$

The wavelength change $\Delta\lambda(n_w, n_o, n_d)$ is for windows 1 and 2 more or less constant along an orbit and from orbit to orbit (except for the mentioned peak values). For window 3 this is not the case: $\Delta\lambda(3, n_o, n_d)$ first decreases with latitude, then increases again, similar to the curve of window 6 shown in Figure 5, with a minimum around -20^o latitude.

As far as the SAA is concerned, the wavelength change for window 2 shows, some distinct peaks in the SAA-region, but on the whole these peaks are somewhat

less pronounced than for window 1, and peaks are also present well outside the SAA, most likely because of the worse signal-to-noise ratio. For window 3 there are some peak values in the SAA-region, but because of the variation along an orbit of $\Delta\lambda(3, n_o, n_d)$, it is not possible to identify the SAA from the wavelength calibration results of window 3.

It should be noted here that $\Delta\lambda(n_w, n_o, n_d)$ does not peak in the same ground pixels for the three windows 1–3 at the same time. The reason for this is that the charged particles which impact when it is over the detector in the SAA-region do so only at random on specific locations of the detector, causing that particular detector pixel to give a peak value, without affecting detector pixels further away.

The impact of these particles is, of course, not limited to wavelength windows 1–3: there are also impacts in the wavelength range beyond window 3. But the radiance levels in these windows is such that the signal-to-noise ratio is large enough to overshadow the effect of a peak-value caused by the impact of a particle, as can be seen from the lack of distinct peaks in the curve of orbit 8 in Figure 4 over the SAA-latitudes.

6. Variations in time of the calibration of solar spectra

The variation in time over several months or years of the wavelength calibration results can be studied from the solar spectra. GOME measures one daily a solar spectrum along one of its orbits when the satellite flies over the North Pole into the sunlight. Solar spectra are measured since the launch of ERS-2 in 1995, and are available in the official product releases of the GDP (mentioned in Section 2.3). These spectra are therefore well suited for an analysis of the long-term variation the wavelength calibration.

The wavelength grid of the GDP solar spectra changes over time and is therefore not suited as initial grid: an analysis of the variation in time of the calibration results requires an initial grid which is the same throughout the period studied. For this reason a constant initial grid is constructed off-line, based on an arbitrary but realistic choice of the initial coefficients for the wavelength windows, as is done for the calibration of the earthshine spectra (Section 2.1).

The data selected for the study presented here are the solar spectra for days 5, 15 and 25 of each month from 5 July 1995 up to and including 5 June 2001 (extracted with version 2.00 of the GDP_01 extractor, without the instrument degradation corrections). Occasionally a solar spectrum is missing, for example due to maintenance of the satellite, leaving in total 205 spectra for a period of just under six years (after 5 June 2001 there are almost no solar spectra available in the GDP data, because of the severe degradation of the instrument). The results of the wavelength calibration are characterised by the wavelength change $\Delta\lambda(n_w)$ of the data point in the middle of window n_w.

The average irradiance level of the GOME spectra shows a decrease in time due to the degradation of the instrument, which appears to be faster for shorter wavelengths.[15,17] Figure 8 shows the average irradiance values in the nine wavelength windows as function of time for the selected solar spectra, plotted relative

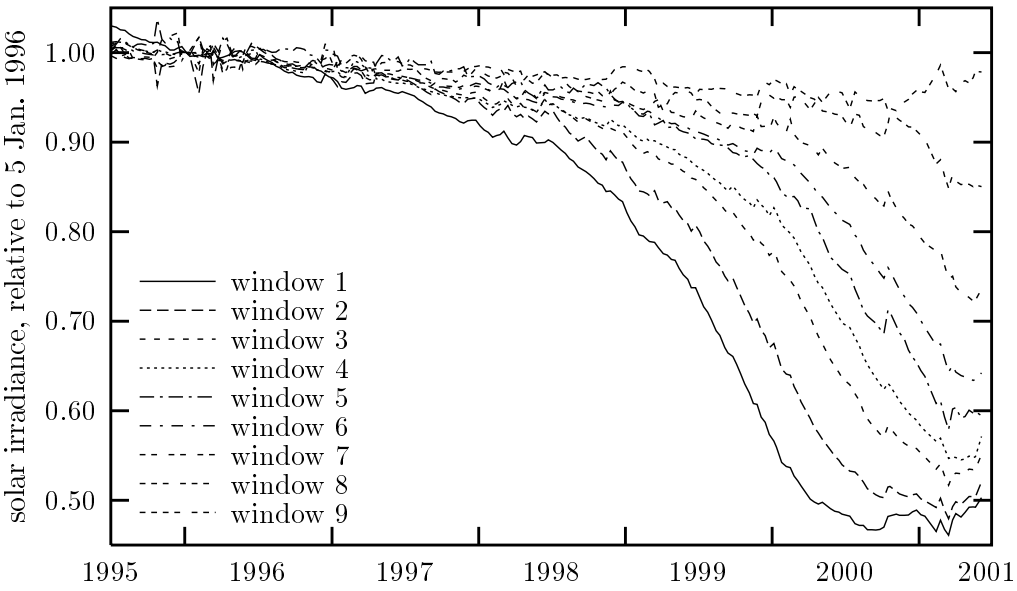

Figure 8 *Average irradiance values of GOME solar spectra in the nine wavelength windows listed in Table 2 over a period of almost six years, plotted relative to the respective values at 5 January 1996. The seasonal variation due to the elliptical form of the Earth's orbit has been corrected for. At the right of the plot, the window number increases from 1 for the bottom curve to 9 for the top curve.*

to the values at 5 January 1996. From the curves in this graph, the degradation of the solar measurements is evident, starting with the shortest wavelengths. During this period the Sun has become more active, because the solar magnetic (sunspot) cycle had a minimum in 1996 and a maximum in 2001. The increase in the intensity of the sunlight in the wavelength range of GOME is less than 1%, hence the increase in solar activity has no visible influence on the curves in Figure 8.

Figure 9 shows the wavelength change $\Delta\lambda(n_w)$ for windows 1 and 6, as an example of the variation in time of the wavelength calibration of solar spectra.

For window 1 there is, on average, a small decrease in $\Delta\lambda(1)$, about 0.001 nm from left to right. This is smaller than the fluctuations in $\Delta\lambda(1)$: the average of $\Delta\lambda(1)$ over the entire period is 0.0012 ± 0.0015 nm. Also, $\Delta\lambda(1)$ shows no correlation with the irradiance level in Figure 8. The variations of $\Delta\lambda(n_w)$ for windows 2–5 (not shown) are similar to $\Delta\lambda(1)$ and there is no correlation with the irradiance level either. The variation of $\Delta\lambda(1)$ plotted in Figure 9 shows many peaks and most of these appear at the same day and in the same direction also in $\Delta\lambda(n_w)$ for windows 2–5.

The variation in the wavelength change for window 6, also plotted in Figure 9, shows a somewhat more pronounced decrease in time than the $\Delta\lambda$ for window 1 does, but mainly in the first two years and within the standard deviation of an average over all $\Delta\lambda(6)$-points (which is 0.0020 nm). The decrease of $\Delta\lambda(n_w)$ with time for windows 7 and 8 (not shown) is even less than the decrease in $\Delta\lambda(6)$. The peaks in $\Delta\lambda(n_w)$ for these three windows in channel 2 are similar in location and magnitude.

The wavelength change for window 9 (not shown), finally, shows a marginal

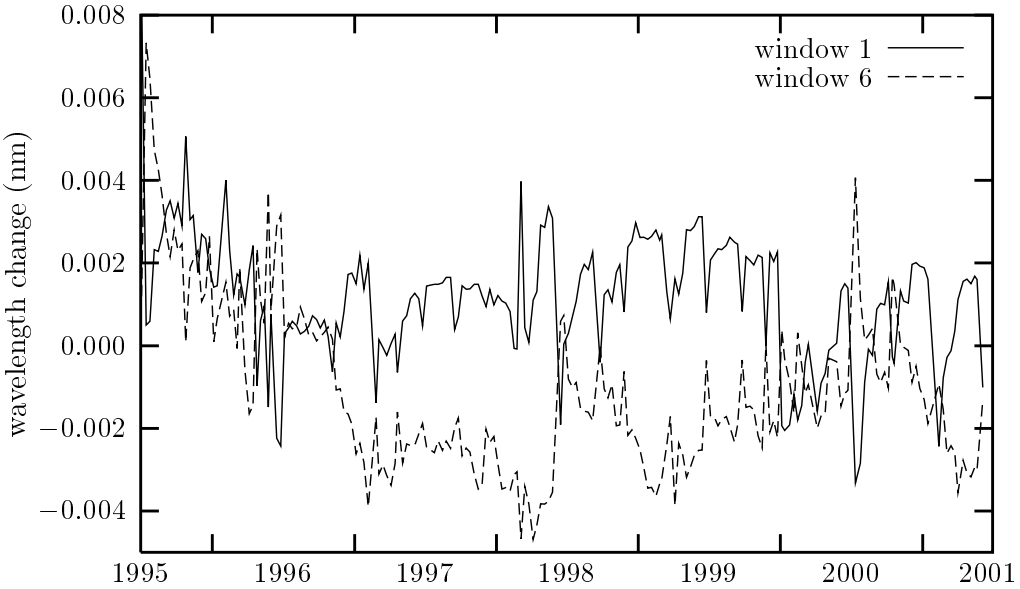

Figure 9 *Wavelength change $\Delta\lambda(n_w)$ as a result of the wavelength calibration in two windows of GOME solar spectra, as function of time. As the calibration starts from different initial grids for the windows, only the change in time of $\Delta\lambda(n_w)$ can be compared, not the absolute values.*

increase with time, much smaller than the standard deviation of the average (0.0034 nm). Peaks in $\Delta\lambda(9)$ appear not to be correlated with peaks in the variations in channels 1 and 2.

As noted, there are several peaks in the variation of $\Delta\lambda(n_w)$ in time without an apparent pattern, except that there seems to be an anti-correlation in the peaks between windows in channels 1 and 2. What causes these peaks, and the anti-correlation, is unknown. The sunlight entering the GOME instrument first passes through a sun diffuser, in order to reduce the intensity of the sunlight so as not to damage the detectors, and it is known that there are wavelength dependent effects in the diffuser (C. Tanzi, private comm.). Further, the calibration of the diffuser is not optimal, because its BSDF (bi-directional scattering distribution function) has not been calibrated well before launch.[20] The largest deviation of the BSDF is in July, which does not correlate with the peaks in Figure 9.

7. Concluding remarks

The present paper investigated the variation of the wavelength calibration of GOME earthshine spectra, *in casu* the wavelength change $\Delta\lambda$ with respect to an initial guess in selected wavelength windows (listed in Table 2), along an orbit and between successive orbits on three days, and a possible correlation with some instrument temperatures. The temperature of some of the elements of the optical system namely show an increase along an orbit due to warming of the instrument. The temperature T of the predisperser prism, the dispersive characteristics of which are expected to be temperature depended, appears to be a good proxy for the warming of the optical system.

For the wavelength window around 306 nm there is a significant correlation between $\Delta\lambda$ and T along a given orbit, though this correlation is less obvious when considering several orbits at a time. The $\Delta\lambda$ of the other selected windows shows no significant correlation with the predisperser prism temperature and the orbital variation is different for the different windows. What the cause is of these orbital variations in the wavelength calibration is therefore unknown.

The calibration results for the window with the lowest wavelengths, around 274 nm, show distinct peaks when the satellite is above the South Atlantic Anomaly (SAA), a region of the inner Van Allen radiation belt where much more charged particles impact on the instrument detector than elsewhere along the orbit. This increase in charged particle impacts on the detector causes spikes in the radiance levels and these spikes in turn hamper the wavelength calibration if the signal-to-noise ratio is not to good, which is the case for the shorter wavelengths of windows below about 300 nm. It is therefore advisable to omit the SAA-region (roughly between latitudes -5° and -40°, and between longitudes -5° and -80°) from the wavelength calibration and adopt, for example, the average results of the calibration between, say, $+5^{\circ}$ and $+30^{\circ}$ latitude of the orbit for the SAA-region.

The wavelength calibration of solar spectra measured over a period of nearly six years shows fluctuations in the change in wavelength $\Delta\lambda$ with time, but without an apparent pattern. The degradation of the GOME instrument, clearly visible in the irradiance levels, has no effect on the wavelength calibration of the solar spectra.

Acknowledgements

The research described in this paper is performed within the framework of the GOME Fast Delivery and Value-Added Products (GOFAP) project, part of ESA's Data User Programme (DUP). The author would like to thank R. van der A, R. van Oss, A. Piters and P. Stammes for useful discussions.

References

1. *The Global Ozone Monitoring Experiment (GOME) Users Manual* SP-1182, European Space Agency, Noordwijk, The Netherlands (1995).
2. A. Hahne, *The Global Ozone Monitoring Experiment* SP-1212, European Space Agency, Noordwijk, The Netherlands (1997).
3. J.P. Burrows, M. Weber, M. Buchwitz, V. Rozanov, A. Ladstätter-Weißenmayer, A. Richter, R. Debeek, R. Hoogen, K. Bramstedt, K.-U. Eichmann, M. Eisinger and D. Perner, "The Global Ozone Monitoring Experiment (GOME): Mission concept and first results," *J. Atmos. Sciences* **56**, no. 2, 151–175 (1999).
4. P.J.M. Valks, A.J.M. Piters, J.C. Lambert and C. Zehner, "Improved near-real time GOME ozone column retrieval," in *Proceedings of the ERS-ENVISAT Symposium: Looking down to Earth in the New Millennium*, SP-461, European Space Agency, Noordwijk, The Netherlands (CD-ROM) (2000).
5. R.J. Van der A, H.J. Eskes, J. Van Geffen, R.F. Van Oss, A.J.M. Piters, P.J.M. Valks and C. Zehner, "GOME Fast dilevery and value-Added Products (GOFAP)," in *Proceedings of the ERS-ENVISAT Symposium: Looking down to Earth in the New Millennium*, SP-461, European Space Agency, Noordwijk, The Netherlands (CD-ROM) (2000).

6. P.J.M. Valks, A.J.M. Piters, J.C. Lambert, C. Zehner and H.M. Kelder, A Fast Delivery system for the retrieval of near-real time ozone columns from GOME data, *Int. J. Remote Sensing* **24**, 423–436 (2003).
7. R.J. Van der A, A.J.M. Piters, R.F. Van Oss, P.J.M.Valks, J.H.G.M. Van Geffen, H.M. Kelder and C. Zehner, "Near-real time delivery of GOME ozone profiles," in *Proceedings of the ERS-ENVISAT Symposium: Looking down to Earth in the New Millennium*, SP-461, European Space Agency, Noordwijk, The Netherlands (CD-ROM) (2000).
8. R.B.A. Koelemeijer, P. Stammes, J.W. Hovenier and J.F. De Haan, "A fast method for retrieval of cloud parameters using oxygen A-band measurements from the Global Ozone Monitoring Experiment," *J. Geophys. Res.* **106**, 3475–4390 (2001).
9. R.B.A. Koelemeijer, P. Stammes, J.W. Hovenier and J.F. De Haan, "Global distribution of effective cloud fraction and cloud top pressure derived from oxygen A band spectra measured by the Global Ozone Monitoring Experiment: Comparison to ISCCP data," *J. Geophys. Res.* **107**, 10.1029/2001JD000840 (2002).
10. A.J.M. Piters, R.J. Van der A, J.H.G.M. Van Geffen, R.F Van Oss and P.J.M. Valks, "Retrieving spectral reflectivities from Extracted GOME Instrument header data," in *Proceedings of the ERS-ENVISAT Symposium: Looking down to Earth in the New Millennium*, SP-461, European Space Agency, Noordwijk, The Netherlands (CD-ROM) (2000).
11. J.H.G.M. Van Geffen and R.F. Van Oss, Wavelength calibration of spectra measured by Global Ozone Monitoring Experiment by use of a high-resolution reference spectrum, *Applied Optics* **42**, 2739–2753 (2003).
12. K. Chance and R.J.D. Spurr, "Ring effect studies: Rayleigh scattering, including molecular parameters for rotational Raman scattering, and the Frounhofer spectrum," *Applied Optics* **36**, 5224–5230 (1997).
13. W. Balzer, B. Aberle, D. Loyola and R. Spurr, "GOME Level 0 to 1 Algorithm Description," *ER-TN-DLR-GO-0022*, Iss./Rev. 4/A, Deutsches Centrum für Luft- und Raumfahrt, Oberpfaffenhofen, Germany (1996).
14. P.K. Bhartia (ed.), *OMI Algorithm Theoretical Basis Document, Volume II, OMI Ozone Products*, OMI-ATBD-02, Version 2.0, NASA Goddard Space Flight Center, Greenbelt, Md. (2002).
15. A. Von Bargen and W. Thomas, "Updated report for GDP 0-to-1 Version 2.0 and GDP 1-to-2 Version 2.7," release by D. Loyola, *ER-TN-DLR-GO-0043*, Iss/Rev.1/A, Deutsches Centrum für Luft- und Raumfahrt, Oberpfaffenhofen, Germany (1999).
16. N.A.J. Schutgens and P. Stammes, "Parametrisation of Earth's polarisation spectrum from 290 to 330 nm," *J. Quantitative Spectroscopy and Radiative Transfer* **75**, 239–255 (2002).
17. R. Van der A, *Recalibration of GOME spectra for the purpose of ozone profile retrieval*, Technical Report TR-236, KNMI, De Bilt, The Netherlands (2001).
18. R.J. Van der A, R.F. Van Oss, A.J.M. Piters, J.P.F. Fortuin, Y.J. Meijer and H.M. Kelder, Ozone profile retrieval from recalibrated Global Ozone Monitoring Experiment data, *J. Geophys. Res.* **107**, 10.1029.2001JD000696 (2002).
19. J.H.G.M. Van Geffen, *Documentation of the software package GomeCal* (version 1.0), Technical report TR-255, KNMI, De Bilt, The Netherlands (2003). [Also available on-line via `http://www.knmi.nl/gome_fd/gomecal/`]
20. I. Aben, M. Eisinger, E. Hegels, R. Snel and C. Tanzi, "GOME Data Quality Improvement," *TN-GDAQI-003SR/2000*, Final Report, Appendix B, Space Research Organisation Netherlands, Utrecht, Netherlands (2000).

Appendix

Section 5 discusses the variation along an orbit of the results of the wavelength calibration of earthshine spectra from 1–3 March 2000, *in casu* the wavelength change of the point in the middle of the wavelength window with respect to the initial wavelength grid: $\Delta\lambda(n_w, n_o, n_d)$, where n_w is the window number (*cf.* Table 2), and n_o the number of the orbit on day n_d in March 2000. Section 5 investigates a possible correlation of this wavelength change with the variation along an orbit of the temperature of the predisperser prism: $T(n_o, n_d)$.

The coefficient of correlation between two data sets X and Y, each with n data points, is given by:

$$C = \frac{n\Sigma(XY) - (\Sigma X)(\Sigma Y)}{\sqrt{\{n\Sigma(X^2) - (\Sigma X)^2\}\{n\Sigma(Y^2) - (\Sigma Y)^2\}}}$$

Let in this case X be the temperature of the predisperser prism $T(n_o, n_d)$ and Y the wavelength change $\Delta\lambda(n_w, n_o, n_d)$, then tables 4, 5 and 6 list the respective correlation coefficients $C(n_w, n_o, n_d)$. The entry "all" refers to taking all orbits of that particular day together in the computaton of the coefficient.

Table 4 *Correlation coefficients $C(n_w, n_o, n_d = 1)$ for 1 March 2000.*

	n_w								
n_o	1	2	3	4	5	6	7	8	9
1	.655	–.101	–.409	–.920	.254	.396	–.035	–.291	.594
2	.673	.096	–.242	–.887	–.055	.322	.083	–.024	.676
3	.717	.076	–.610	–.922	–.123	.320	.233	–.033	.497
4	.192	.709	–.402	–.840	–.361	–.090	.553	–.330	.708
5	.377	–.850	–.800	–.944	–.631	.306	–.073	–.388	.420
6	.224	.387	–.562	–.942	–.023	–.121	–.014	–.254	.505
7	.161	–.027	–.391	–.927	–.269	.215	–.316	–.691	.307
8	–.091	–.100	–.445	–.903	–.441	–.264	–.435	–.735	.346
9	.376	–.181	–.043	–.953	–.530	.336	–.069	–.523	.636
10	.195	.434	–.373	–.924	–.322	.142	–.165	.125	.628
11	.763	.411	–.672	–.967	–.387	.710	.090	–.769	.789
12	.458	.692	–.646	–.947	–.212	–.322	.158	.171	–.007
13	.561	–.792	–.478	–.969	.016	.469	–.244	–.850	–.117
14	.568	–.243	–.673	–.930	–.269	.097	–.054	–.464	.442
all	.148	–.065	–.296	–.762	–.055	.144	.070	–.164	.365

Table 5 *Correlation coefficients $C(n_w, n_o, n_d = 2)$ for 2 March 2000. Note: the unusually small correlation coefficient for $n_w = 4$ and $n_o = 1$ with respect to the coefficients for the same window in all other orbits of the three days may be due to an error in the EGOI data file.*

	n_w								
n_o	1	2	3	4	5	6	7	8	9
1	–.034	.235	–.845	–.024	.063	.561	–.458	–.033	.890
2	.807	.442	–.235	–.649	–.212	.296	–.046	–.223	.425
3	.455	.249	–.453	–.720	–.297	.289	.185	.013	.370
4	.506	.324	–.805	–.833	–.312	.201	.114	–.361	.334
5	–.195	–.051	–.648	–.959	–.306	.139	–.210	–.291	.007
6	.277	.563	–.636	–.938	–.313	.308	–.056	–.624	.307
7	.292	.012	–.522	–.938	–.012	.275	–.221	–.550	.550
8	.017	–.243	–.433	–.925	–.643	.040	–.370	–.698	.424
9	–.199	–.279	–.179	–.939	–.637	.292	–.091	–.389	.692
10	.401	.361	–.486	–.941	–.609	.651	.008	–.824	.334
11	.151	–.027	–.665	–.935	–.306	–.223	–.090	.043	.147
12	–.240	.395	–.054	–.931	–.297	–.056	.342	–.433	–.475
13	.344	–.350	–.689	–.957	–.094	.584	–.437	–.431	.758
14	–.104	.138	–.702	–.902	–.182	.393	–.162	–.453	.489
15	.083	–.061	–.548	–.795	.037	.644	–.170	–.344	.517
all	.098	–.040	–.288	–.597	–.078	.137	.012	–.196	.298

Table 6 *Correlation coefficients $C(n_w, n_o, n_d = 3)$ for 3 March 2000.*

	n_w								
n_o	1	2	3	4	5	6	7	8	9
1	.775	–.017	–.421	–.649	–.161	.817	–.153	–.266	.603
2	.612	–.190	–.242	–.762	–.297	.776	.124	–.271	.625
3	.487	–.531	–.511	–.890	–.477	.652	–.028	–.441	.426
4	.383	–.381	.386	–.885	–.963	.805	–.173	.896	.726
5	.641	–.099	–.524	–.908	–.221	.355	.157	–.608	.047
6	.148	.243	–.784	–.951	–.167	.260	–.347	–.675	.371
7	–.182	.368	–.524	–.953	–.547	–.026	–.193	–.535	.419
8	–.118	–.306	–.527	–.925	–.234	.223	–.460	–.287	.480
9	.185	–.318	–.409	–.928	–.005	.349	.252	–.794	.340
10	.202	.544	.019	–.893	–.427	–.641	.061	.110	–.411
11	.153	–.315	–.810	–.926	.410	.507	–.270	–.199	.770
12	.489	.879	–.807	–.964	–.277	.690	–.700	–.719	.909
13	.308	–.478	–.508	–.947	–.156	.116	–.257	–.505	.256
14	.094	–.133	.023	–.918	.132	–.053	–.432	–.566	.508
all	–.007	.019	–.300	–.714	–.118	.198	–.062	–.257	.304